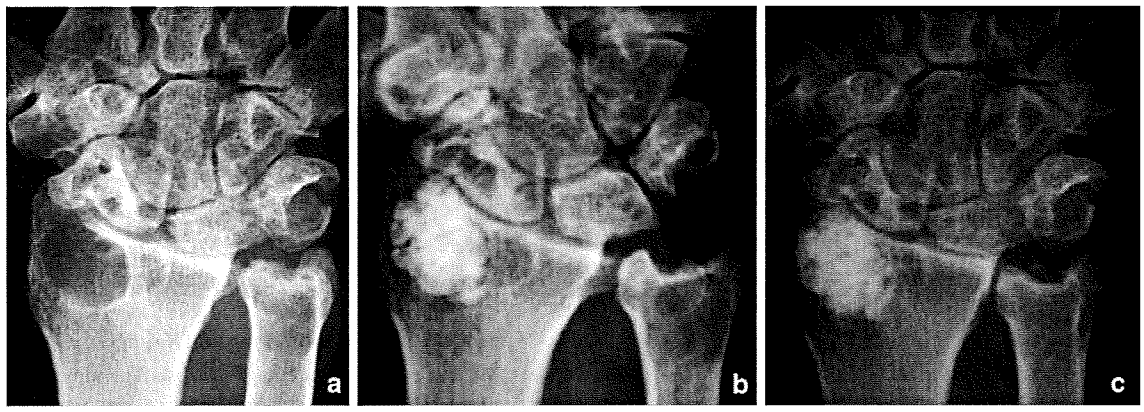

Fig. 2 Case 6: **a** preoperative radiograph reveals a large radiolucent area in the distal radius. **b** Appearance just after surgery. **c** At 37 months after surgery, there is no absorption of IP-CHA or expansion of the cystic lesion

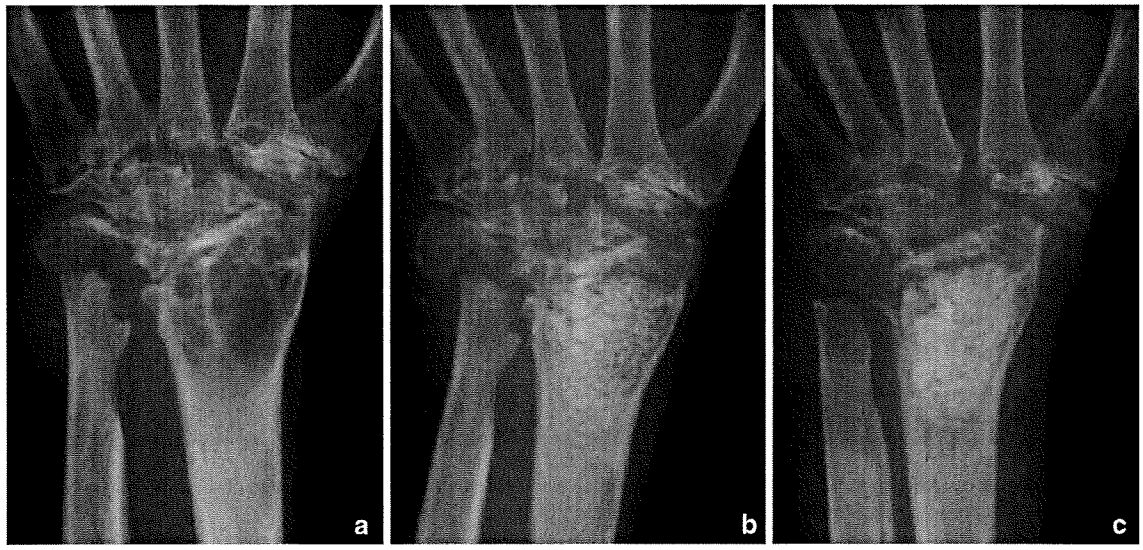

Fig. 3 Case 7: **a** preoperative radiograph reveals a large radiolucent area in the distal radius. **b** Appearance just after the operation. Curettage and IP-CHA implantation are inadequate. **c** At 16 months after surgery, there is expansion of the cystic lesion, but no reabsorption of implanted IP-CHA

and expansion of the cystic lesion occurred with appearance of a radiolucent zone around the implanted IP-CHA at final follow-up (Fig. 3).

Before surgery, cases 5 and 9 had pain and swelling of the wrist. Their pain and swelling improved after synovectomy in addition to curettage and packing of the lesions. In case 2 (Fig. 1), preoperative knee joint pain was improved after curettage of a tibial cystic lesion and packing with IP-CHA, as well as synovectomy of the knee joint. The range of joint motion did not change significantly after surgery. There were no complications related to implanting IP-CHA, such as excessive postoperative drainage, erythema, or wound infection.

Discussion

Juxta-articular intraosseous cystic lesions are commonly found during the course of RA, and these lesions can cause spontaneous pathological fractures that result in extensive joint destruction [5–8]. Nakagawa et al. reported two cases of giant geodes involving the olecranon process. They performed surgery for an associated pathological fracture in one patient and treated the other patient prophylactically with an autologous iliac bone graft to prevent fracture [5]. Lowthian et al. reported a patient who had multiple pathological fractures of the phalanges due to cystic lesions that led to residual instability of the

fingers despite surgical treatment [6]. Wordsworth et al. reported a patient with a pathological fracture of the proximal ulna that was initially treated conservatively but failed to unite, so that bone grafting was subsequently performed [7]. Rappoport et al. reported three patients with chronic RA who developed pathological fractures of the olecranon process due to erosions or cysts [8]. Although intraosseous cystic lesions often occur in patients with active RA and wrist joint involvement, it is difficult to detect such lesions associated with fracture of the distal radius by either clinical or radiographic assessment. One reason might be that intermittent radiological evaluation does not allow detection of pathological fracture of the subchondral bone associated with an intraosseous cystic lesion. The second reason might be that concomitant pathological changes, including erosions, destruction of cartilage, and subluxation of the radiocarpal joint, make it difficult to detect an intraosseous cystic lesion associated with fracture of the distal radius. In one of our patients, joint collapse was associated with the cystic lesion on radiographs. Figure 4a shows a double contour indicating a fracture adjacent to this patient's intraosseous cystic lesion, while Fig. 4b displays rapid progression of joint destruction after six months. Once joint destruction has occurred (as in Fig. 4b), it is quite difficult to detect the presence of a cystic lesion near the radiocarpal joint. The findings in this patient suggest that prophylactic surgical treatment of juxta-articular intraosseous cystic lesions in RA patients could be useful to prevent impending fracture, as is the case with benign bone tumors like solitary bone cyst or giant cell tumor of bone. However, surgery is not often performed in RA patients for the following reasons (among others). First, a juxta-articular intraosseous cystic lesion causes no symptoms or inconvenience itself. Second, autologous bone grafting is associated with donor site morbidity [13], and there are limitations on grafting because of the possible need for multiple operations in patients with RA. Third, an artificial bone substitute with excellent bone conduction properties was not available in the past. Conventional hydroxyapatite implants achieve little bone ingrowth into the deeper regions because there are few interpore connections allowing bone marrow cells to infiltrate into the implant, so a hydroxyapatite implant does not gain sufficient mechanical strength. On the other hand, IP-CHA has demonstrated excellent osteoconductivity in animal models as well as in clinical trials [9, 14]. IP-CHA has a high porosity (75%), and the pores show uniform connections with each other like the pores in cancellous bone. The majority of the pores are approximately 100–200 μm in diameter with interconnections that are about 40 μm in diameter, and the compression strength of IP-CHA is about 10 MPa [14]. These structural differences from conventional hydroxyapatite confer excellent bone conduction, so that host bone ingrowth is sufficient to achieve adequate mechanical strength without autologous bone grafting. On the other hand, Suzuki et al. reported a patient with a giant geode in the tibial condyle that was successfully treated with calcium phosphate cement (CPC) [15]. Although the use of CPC provides initial high mechanical strength and incorporation of the implant surface into host bone may occur, a CPC block has no pores. IP-CHA provides sufficient mechanical strength after new bone ingrowth occurs due to its cancellous

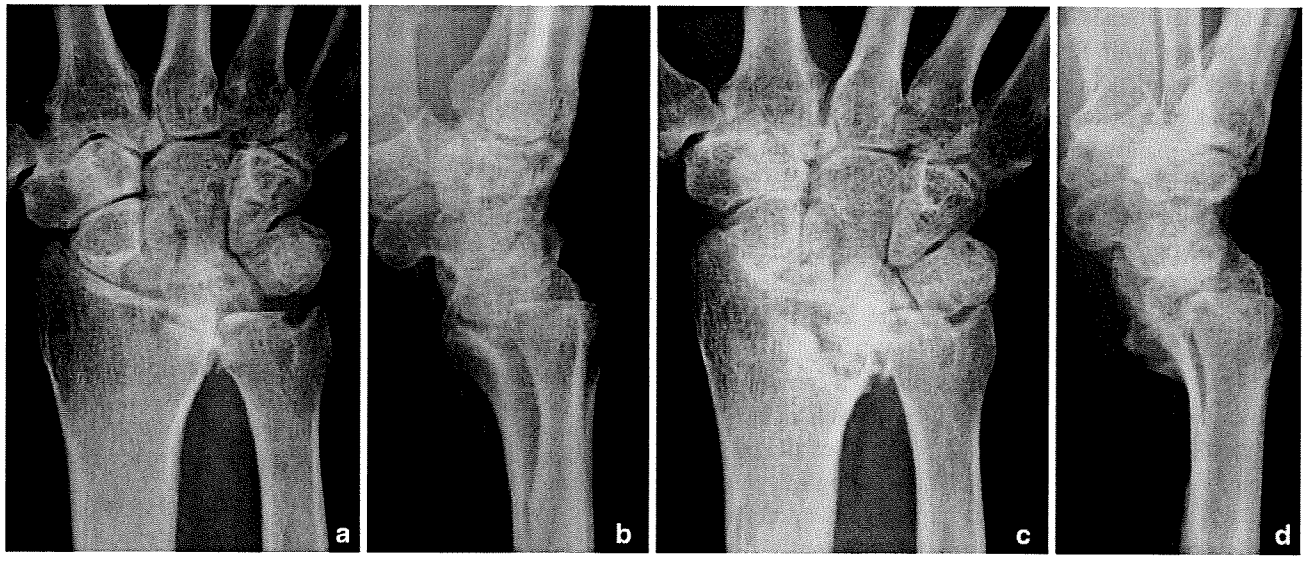

Fig. 4 A 54-year-old man: **a**, **b** there is a pathological fracture and cystic lesion of the lunate fossa in the distal radius. **c**, **d** After 6 months, joint destruction shows marked progression

structure, and it might also show more physiological resistance to mechanical stress. We aimed to utilize these properties of IP-CHA to improve mechanical strength in the treatment of intraosseous cystic lesions, and achieved good radiological results in the present series. We also found that IP-CHA is easy to handle and there is little risk of leakage into adjacent joints.

In patients with RA, the bone adjacent to involved joints develops juxta-articular osteoporosis, erosions, and intraosseous cystic lesions, with these changes being considered to be due to an increase of osteoclastic bone resorption [16–19] secondary to local overproduction of bone-resorbing cytokines. The present study revealed that IP-CHA was resistant to absorption, even in the pathological state of RA for at least 47 months after surgery. This property of IP-CHA makes it suitable for treating RA because a more biodegradable material could also be remodeled into bone but might then be affected by juxta-articular osteoporosis or erosive changes.

One of our patients had severe RA that could not be controlled due to concomitant hepatic and pancreatic dysfunction. The CRP level of this patient remained above 2.0 mg/dl before and after surgery, and expansion of the cystic lesion occurred despite surgical treatment. This case suggests that curettage and implantation of IP-CHA will not suppress local disease activity and prevent the expansion of a lesion if the patient has poorly controlled RA. Recent advances in the treatment of RA with the advent of biological agents have made it possible to prevent the progression of joint destruction [20, 21]. Accordingly, the expansion of cystic lesions may also be prevented by controlling disease activity with more effective drugs. Such advances in medical therapy may allow curettage and packing with IP-CHA to become a better treatment for juxta-articular intraosseous cystic lesions.

In patients with RA, the goals of surgical treatment include relief of pain and improvement of joint function. Procedures such as synovectomy, arthrodesis, and resection arthroplasty mainly target pain relief. Implant arthroplasty targets both pain relief and functional improvement, while tendon transfer and tendon grafting are procedures that aim to improve function. The present procedure represents a new category of surgical treatment for RA that is indicated to prevent impending articular fracture due to a large intraosseous cystic lesion.

In RA patients, joint destruction is a process that involves several events, including destruction of the surface cartilage, resorption of mineralized cartilage, and erosion of subchondral bone [22]. Pathological fracture associated with a juxta-articular intraosseous cystic lesion can also contribute to joint destruction, but not all cystic lesions will cause fractures. The size and location of a lesion, as well as juxta-articular osteoporosis, marginal sclerosis, systemic disease activity, and the local inflammatory response might all influence the risk of fracture. To adequately decide the indications for this procedure, a method for assessing the risk of impending fracture associated with juxta-articular intraosseous cystic lesions is the next issue to be clarified. Recently, we have been evaluating the impending fracture with CT, which shows the size, location and features of a lesion clearly (see Fig. 1 in the "Electronic supplementary material"). Limitations of the present study include the small number of subjects and the lack of a control group. However, these preliminary results are still encouraging and suggest that treatment with IP-CHA may become a useful method for preventing fracture associated with juxta-articular intraosseous cystic lesions in RA patients.

Conflict of interest statement The authors declare that there are no competing financial interests.

References

1. Crane AR, Scarano JT. Synovial cysts (ganglia) of bone. J Bone Joint Surg Am. 1967;49:355–61.
2. Harrison MHM, Schajowicz F, Trueta J. Osteoarthritis of the hip and study of the nature and evolution of the disease. J Bone Joint Surg Br. 1953;35:598–626.
3. Cruickshank B, Macleod IG, Shearer WS. Subarticular pseudocysts in rheumatoid arthritis. J Fac Radiol. 1954;5:218–26.
4. Resnick D, Niwayama G, Coutts RD. Subchondral cysts (geodes) in arthritic disorders: pathologic and radiographic appearance of the hip joint. Am J Roentgenol. 1977;128:799–806.
5. Nakagawa N, Abe S, Saegusa Y, Kimura H, Imura S, Nishibayashi Y, et al. Giant geode at the olecranon in the rheumatoid elbow—two case reports. Clin Rheumatol. 2004;23:358–61.
6. Lowthian PJ, Calin A. Geode development and multiple fractures in rheumatoid arthritis. Ann Rheum Dis. 1985;44:130–3.
7. Wordsworth BP, Mowat AG, Watson NA. Fracture through a geode in the proximal ulna. Br J Rheumatol. 1984;23:110–2.
8. Rappoport AS, Sosman JL, Weissman BN. Spontaneous fractures of the olecranon process in rheumatoid arthritis. Radiology. 1976;119:83–4.
9. Myoui A, Tamai N, Nishikawa M, Yoshikawa H, Araki N, Nakase T, et al. Three-dimensionally engineered hydroxyapatite ceramics with interconnected pores as a bone substitute and tissue engineering scaffold. Biomater Orthop. 2003;13:287–300.
10. Arnett FC, Edworthy SM, Bloch DA, McShane DJ, Fries JF, Cooper NS, et al. The American Rheumatism Association 1987 revised criteria for the classification of rheumatoid arthritis. Arthritis Rheum. 1988;31:315–24.
11. Steinbrocker O, Traeger GH, Batterman RC. Therapeutic criteria in rheumatoid arthritis. J Am Med Assoc. 1949;140:659–62.
12. Larsen A, Dale K, Eek M. Radiographic evaluation of rheumatoid arthritis and related conditions by standard reference films. Acta Radiol Diagn. 1977;18:481–91.
13. Goulet JA, Senunas LE, DeSilva GL, Greenfield ML. Autogenous iliac crest bone graft. Complications and functional assessment. Clin Orthop Relat Res. 1997;339:76–81.
14. Tamai N, Myoui A, Tomita T, Nakase T, Tanaka J, Ochi T, et al. Novel hydroxyapatite ceramics with an interconnective porous

structure exhibit superior osteoconduction in vivo. J Biomed Mater Res. 2002;59:110–7.
15. Suzuki M, Kim T, Tamai H, Fujiyoshi T, Moriya H. Giant geode treated with calcium phosphate cement in a rheumatoid knee. J Rheumatol. 2005;32:1846–8.
16. Bromley M, Woolley DE. Chondroclasts and osteoclasts at subchondral sites of erosion in the rheumatoid joint. Arthritis Rheum. 1984;27:968–75.
17. Gravallese EM, Harada Y, Wang JT, Gorn AH, Thornhill TS, Goldring SR. Identification of cell types responsible for bone resorption in rheumatoid arthritis and juvenile rheumatoid arthritis. Am J Pathol. 1998;152:943–51.
18. Kong YY, Feige U, Sarosi I, Bolon B, Tafuri A, Morony S, et al. Activated T cells regulate bone loss and joint destruction in adjuvant arthritis through osteoprotegerin ligand. Nature. 1999;402:304–9.
19. Gravallese EM, Manning C, Tsay A, Naito A, Pan C, Amento E, et al. Synovial tissue in rheumatoid arthritis is a source of osteoclast differentiation factor. Arthritis Rheum. 2000;43:250–8.
20. van der Heijde D, Landewe R, Klareskog L, Rodriguez-Valverde V, Settas L, Pedersen R, et al. Presentation and analysis of data on radiographic outcome in clinical trials: experience from the TEMPO study. Arthritis Rheum. 2005;52:49–60.
21. Genovese MC, Bathon JM, Fleischmann RM, Moreland LW, Martin RW, Whitmore JB, et al. Long-term safety, efficacy, and radiographic outcome with etanercept treatment in patients with early rheumatoid arthritis. J Rheumatol. 2005;32:1232–42.
22. Schett G. Erosive arthritis. Arthritis Res Ther. 2007;9(Suppl 1):S2.

SCIENTIFIC ARTICLE

Interosseous Membrane of the Forearm: Length Change of Ligaments During Forearm Rotation

Hisao Moritomo, MD, PhD, Kazuo Noda, MD, Akira Goto, MD, PhD, Tsuyoshi Murase, MD, PhD, Hideki Yoshikawa, MD, PhD, Kazuomi Sugamoto, MD, PhD

Purpose An earlier anatomic study described five ligamentous components in the interosseous membrane of the forearm (central band, accessory band, distal oblique bundle, proximal oblique cord, and dorsal oblique accessory cord) and provided their precise location of attachment. In the present study, we investigated *in vivo* length changes of these five ligaments during forearm rotation to understand the function of each ligament.

Methods We acquired computed tomographies of nine forearms from seven healthy volunteers for 3 rotation positions: maximum pronation, neutral position, and maximum supination. We created 3-dimensional models of the radius, ulna, and the 5 ligaments by combining osseous images and anatomic data of ligament attachment. We calculated 3-dimensional ligament lengths between attachments during forearm rotation using a markerless bone registration technique. We also examined relationships between the axis of forearm rotation and each ligament.

Results The distal 3 ligaments (central band, accessory band, and distal oblique bundle) had little change in length during forearm rotation, with their ulnar attachments located almost on the axis of forearm rotation. The 2 proximal ligaments (proximal oblique cord and dorsal oblique accessory cord) changed substantially in length, with their attachments out of the course of the axis.

Conclusions The distal 3 ligaments of the interosseous membrane are essentially isometric stabilizers of the forearm. The distal oblique bundle in the distal membranous portion may stabilize the distal radioulnar joint in 40% of human subjects who have this ligament. *(J Hand Surg 2009;34A:685–691. © 2009 Published by Elsevier Inc. on behalf of the American Society for Surgery of the Hand.)*

Key words Axis of rotation, length, ligament, interosseous membrane, *in vivo*.

THE INTEROSSEOUS MEMBRANE (IOM) of the forearm is a combination of ligaments and membranes that connect the radius to the ulna.[1–3] The IOM is divided into 3 parts: the middle ligamentous complex and the distal and proximal membranous portions on either side of the middle ligamentous complex. The central part of the middle ligamentous complex is called the central band (CB)[1,5] (Fig. 1) and represents the widest and stoutest ligament in the IOM. The CB originates from the interosseous crest of the radius, which is the ridge of the radius that projects toward the ulna, courses distally, and inserts into the interosseous border of the ulna. The remaining ligament adjacent to the CB in the middle ligamentous complex is the accessory band (AB), which forms a thinner ligament than CB.[1] Fibers of the AB run in a alignment similar to the CB.

The proximal membranous portion has 2 ligaments: the proximal oblique cord[2,6–9] and the dorsal oblique

From the Department of Orthopaedic Surgery, Osaka University, Suita, Osaka, Japan.

Received for publication April 18, 2008; accepted in revised form January 13, 2009.

No benefits in any form have been received or will be received related directly or indirectly to the subject of this article.

Corresponding author: Hisao Moritomo, MD, PhD, 2-2 Yamadaoka, Suita, Osaka 565-0871, Japan; e-mail: moritomo@ort.med.osaka-u.ac.jp.

0363-5023/09/34A04-0012$36.00/0
doi:10.1016/j.jhsa.2009.01.015

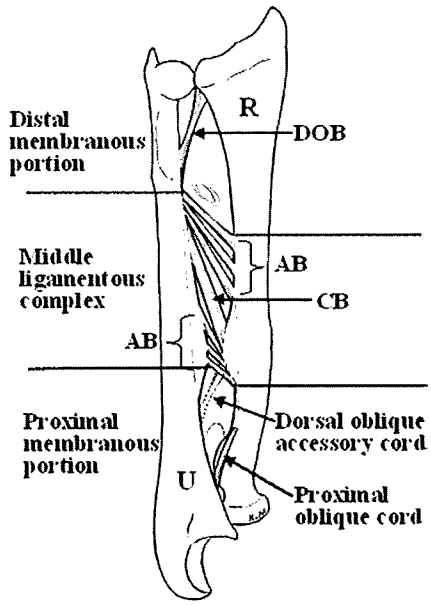

FIGURE 1: Schematic structure of the interosseous membrane. Right forearm view from the anterior aspect. IOM consists of distal, middle, and proximal portions. The middle portion is a ligamentous complex that is further divisible into the CB and AB. The DOB is present within the distal membranous portion. The proximal oblique cord is present on the anterior side of the forearm, and the dorsal oblique accessory cord on the posterior side in the proximal membranous portion. R, radius; U, ulna.

accessory cord[2] (Fig. 1). The proximal oblique cord originates from the anterolateral aspect of the coronoid process of the ulna and inserts just distal to the radial tuberosity. The dorsal oblique accessory cord is exclusively on the dorsal aspect of the forearm, which originates from around the distal two thirds of the ulnar shaft and inserts into the interosseous crest of the radius.

Little attention has been paid to the ligamentous component in the distal membranous portion. Some investigators suggested that the distal membranous portion stabilizes the distal radioulnar joint (DRUJ) when the triangular fibrocartilage complex (TFCC) is disrupted,[10,11] but the exact fiber responsible for this function has not been described. Our preceding anatomic study of the IOM[4] revealed that 12 of 30 cadavers displayed a thick fiber in the distal membranous portion, that is, the distal oblique bundle (DOB), which originated from around the distal one sixth of the ulnar shaft and inserted into the inferior rim of the sigmoid notch of the radius (Fig. 1). We speculated that the DOB, if it exists, may be an important stabilizer of the DRUJ because of its close anatomic relationship with the DRUJ and TFCC.

Functions of the IOM are attributable to an ingeniously arranged structure that allows concurrent smooth forearm rotation and stabilization between the radius and ulna.[5,12] During forearm rotation, each IOM ligament behaves individually, becoming either taut or slack. Measuring the force and tension on each ligament *in vivo* is a useful way to understand how the IOM stabilizes the forearm. Most information regarding the function of the IOM ligamentous complex has been acquired in cadavers using invasive procedures. Such *in vitro* experiments cannot completely reproduce the physical muscular force exerted across the forearm joint *in vivo*. This limitation could alter the normal kinematics of ligaments.

Direct measurement of the force and tension on a ligament *in vivo* is not possible, but researchers have been able to measure *in vivo* kinematics of human joints[13–15] and ligament length[16,17] using noninvasive techniques. We speculated that increased length may indirectly reflect a ligament that is not sagging and is restraining excessive motion, whereas reduced length represents a slackened ligament that does not stabilize motion. Accordingly, length changes in each IOM ligament may partially reflect its function. A previous anatomic study[4] described five ligamentous components in the interosseous membrane of the forearm (the CB, AB, DOB, proximal oblique cord, and dorsal oblique accessory cord) and provided their precise location of attachment, enabling measurement of the change in length of each ligament *in vivo*. We investigated *in vivo* length changes of IOM ligaments during forearm rotation to understand their function.

MATERIALS AND METHODS

Subject preparation and image acquisition

We studied 9 forearms (6 right and 3 left) from 7 healthy volunteers (3 women and 4 men). Mean age was 18.0 years (range, 5–31 years). All subjects provided written informed consent to participate in this study.

Subjects were positioned prone with the arm elevated anteriorly on a computed tomography scanning table (Helical computed tomography; LightSpeed Ultra16; General Electric, Maukesha, WI). Computed tomography images were obtained, with a slice thickness of 1.25 mm, for 3 rotation positions of the forearm: neutral position, maximum supination, and maximum pronation. Maximum position was defined as an extreme position in pronation or supination in which the subject could maintain the position easily without active muscle contraction. The average degree of pronation and supination was 77° ± 15° and 72° ± 10°, respectively. Data were saved in digital imaging and communication in medicine (DICOM) format.

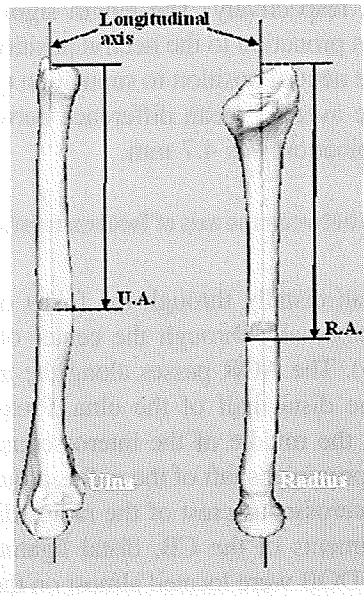

FIGURE 2: Determination of attachment location of IOM ligaments. Location of the center of attachment is expressed as a percentage of total bone length from the distal end of each bone. First, the 3D bone model cut at a plane perpendicular to the longitudinal axis at the level of attachment according to the anatomic data. Then, an attachment point was placed on the interosseous border of the bone. R.A., radial attachment of the ligament; U.A., ulnar attachment of the ligament.

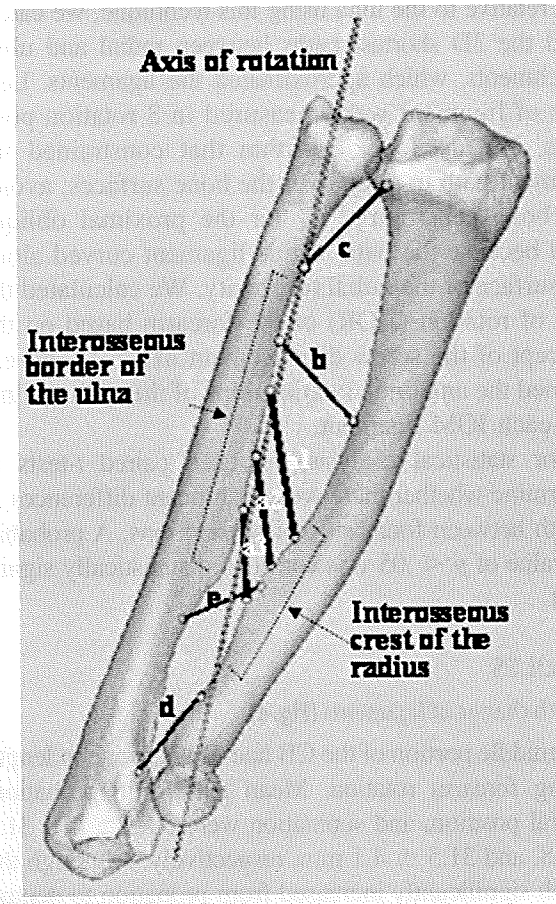

FIGURE 3: Ligament models and the axis of forearm rotation. Right forearm in the neutral position viewed from anterior aspect. a1, distal portion of the central band; a2, middle portion; a3, proximal portion; b, distal ligament of the accessory band; c, distal oblique bundle; d, proximal oblique cord; e, dorsal oblique accessory cord.

Creation of 3-dimensional (3D) models of the radius and ulna

Volumetric data of the forearm were transferred to kinematic analysis software (Virtual Place-M; AZE, Tokyo, Japan) and regions of the radius and ulna in all slice images were extracted semiautomatically by segmentation. We then created 3D models of the radius and ulna from the segmentation data. These models were visualized using software developed in our laboratory (Orthopaedics Viewer; Osaka University, Osaka, Japan).

Determination of attachment locations of IOM ligaments

We calculated the geometric center of mass and the principal axes of inertia for each 3D volume of the radius and ulna. The principal axes of inertia were defined as the long axis, and were placed on radius and ulna models (Fig. 2). Our earlier anatomic study investigated attachment locations of the five ligaments in which the location of the center of the attachment was expressed as a percentage of total bone length from the distal end of each bone. First, we cut the 3D bone model at a plane perpendicular to the longitudinal axis at the level of attachment according to anatomic data. We then placed an attachment point on the interosseous border of the bone. Ligament attachment is not a single point but rather a surface area, and investigating all points in a given area is not possible. We therefore chose a center point for the four ligaments other than the CB. Three points were chosen for the CB (the distal, middle, and proximal portions) because it is a wide ligament (mean width of 9.7 mm)[4] compared with other ligaments.

In vivo measurement of the length of the ligament path

We included five ligaments for length measurement (Fig. 3): the CB, distal ligament of AB, DOB, proximal oblique cord, and dorsal oblique accessory cord. We used a volume-based registration technique[13] to measure ligament length at 3 rotation positions. This technique allows mathematical descriptions of the motion of individual bones and relative motions by superimposing a bone in one position on the other position based on similarity measures. By describing radius mo-

tion relative to the ulna using this technique, we calculated the 3D shortest paths between radial and ulnar attachments, which approximated the ligaments. Lengths of ligament were measured in 3 rotation positions. We used an algorithm that constrained the ligament path to wrap over the bone surfaces, avoiding bone penetration[16,17] for the proximal oblique cord because the path of this ligament curved along the surface of the radial tuberosity. We calculated the axis of rotation (AOR) of the forearm based on the concept of the screw displacement axis[18,19] and examined the anatomic relationships of the radius, ulna, and each IOM ligament.

For statistical analysis, we used paired *t*-tests to determine whether there were significant differences in length between forearm rotation positions. A probability value of $p < .05$ was considered statistically significant.

RESULTS

Length change of ligaments (Fig. 4)

The middle portion of the CB had little change in length during forearm rotation. Mean lengths in pronation, neutral position, and supination were 30.8 ± 4.1, 31.4 ± 3.8, and 31.5 ± 4.1 mm, respectively. Although the length significantly increased from pronation to neutral position ($p < .01$), the mean difference was 0.7 mm. Proximal and distal portions of the CB showed a similar behavioral tendency to the middle portion.

The AB also changed little in length. Mean lengths in pronation, neutral position, and supination were 20.5 ± 2.8, 22.5 ± 3.0, and 22.6 ± 3.3 mm, respectively. The length significantly increased from pronation to the neutral position ($p < .005$) in which the mean difference was 2.1 mm.

The DOB also changed little in length. Mean lengths in pronation, neutral position, and supination were 25.9 ± 3.0, 26.0 ± 3.4, and 25.4 ± 3.1 mm, respectively. Although the length significantly increased from pronation to the neutral position ($p < .01$), the mean difference was only 0.6 mm. The length change of the DOB was the smallest among the five ligaments investigated.

The proximal oblique cord changed substantially in length. Mean lengths in pronation, neutral position, and supination were 30.6 ± 5.4, 26.5 ± 4.7, and 26.4 ± 4.2 mm, respectively. The length significantly decreased from pronation to the neutral position ($p < .0001$) in which the average mean difference was 4.2 mm.

The dorsal oblique accessory cord changed substantially in length. Mean lengths in pronation, neutral position, and supination were 29.2 ± 4.7, 28.2 ± 4.6, and 24.5 ± 3.8, respectively. The length significantly decreased from pronation to the neutral position ($p < .05$) and from the neutral position to supination ($p < .0001$), in which the average mean difference between pronation and supination was 4.7 mm.

Relationships between the axis of forearm rotation and each ligament

The AOR ran distally through the fovea of the ulnar head and proximally through the center of the radial head (Fig. 3). The AOR passes along the interosseous border of the distal half of the ulna. Proximally, the AOR ran in the middle of the interosseous space and through the proximal shaft of the radius around the area where the interosseous crest of the radius disappeared. Ulnar attachments of the CB, distal ligaments of the AB, and the DOB were located almost on the course of the AOR, which suggests that these three ligaments are almost isometric during forearm rotation. Attachments of the proximal oblique cord and dorsal oblique accessory cord were not along the course of the AOR. Relationships of the AOR with the radius, ulna, and each IOM ligament were identical for all nine forearms.

In summary, the distal three ligaments (CB, AB, and DOB) changed little in length during forearm rotation, with their ulnar attachments located almost upon the AOR. The 2 proximal ligaments (proximal oblique cord and dorsal oblique accessory cord) substantially changed in length, with their attachments out of the course of the AOR.

DISCUSSION

Two cadaveric studies have shown the relationship of the AOR to IOM ligaments.[6,12] Mori[6] described the AOR as coinciding with the interosseous border of the ulna, the site of CB insertion. Hollister et al.[12] demonstrated that all thick fibers of the IOM crossed the AOR near insertions in the ulna. Both studies indicate that the CB is an isometric ligament of the IOM with no change in tension during forearm rotation. However, there has been little or no discussion of length change of IOM ligaments other than for the CB.

We found that the CB, AB, and DOB were almost isometric during forearm rotation, although a slight reduction in length occurred in pronation. Nakamura et al.[20–22] carried out *in vivo* studies investigating dynamic changes in the shape of the IOM during forearm rotation using 3D magnetic resonance imaging. They reported that shape deformity in the distal portion of the IOM occurred in pronation owing to muscle contraction of the pronator quadratus muscle. The effect of the

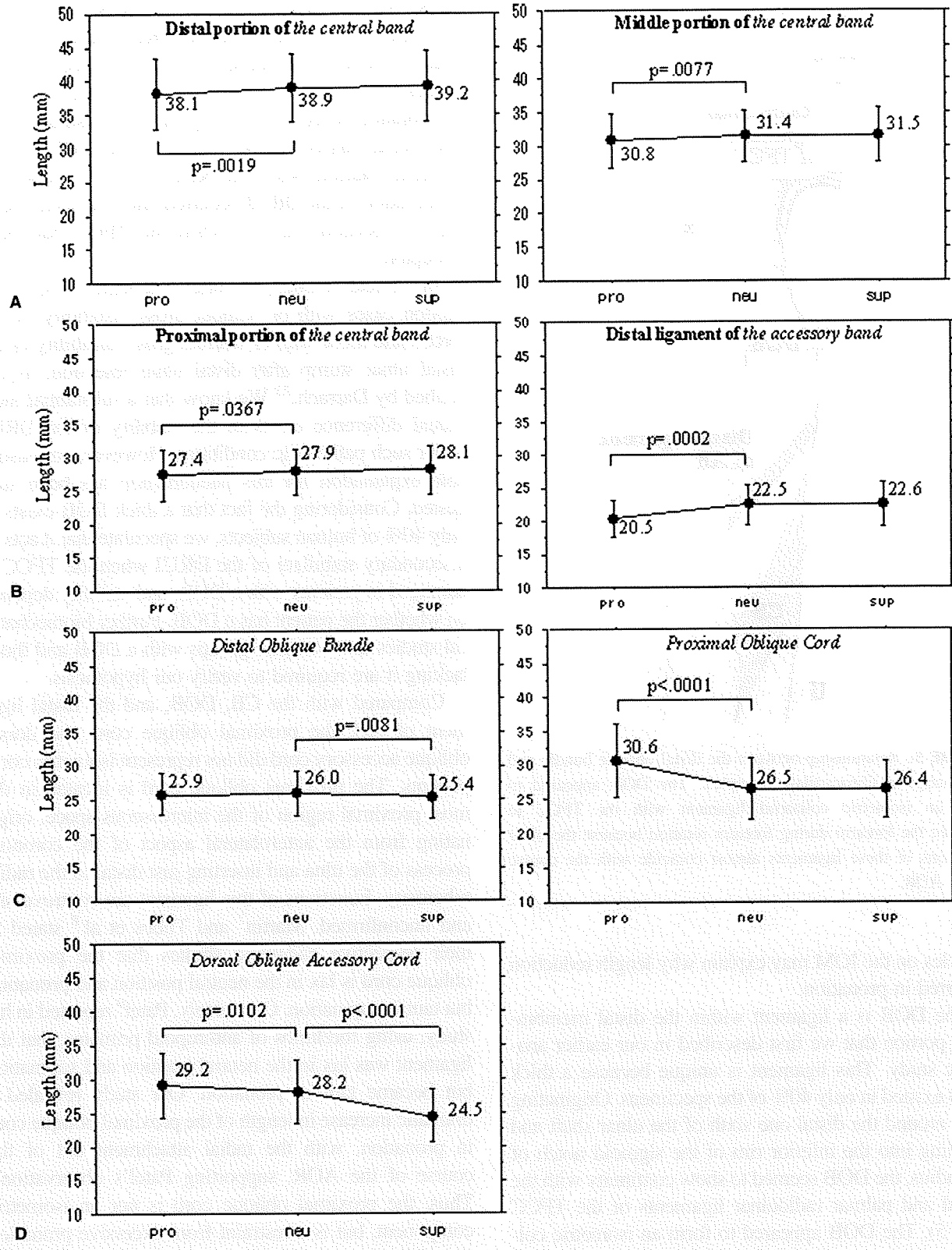

FIGURE 4: A–D Length changes of each IOM ligament. The distal 3 ligaments (CB, AB, and DOB) had little change in length during forearm rotation. In comparison, the proximal 2 components (proximal oblique cord and dorsal oblique accessory cord) changed substantially in length.

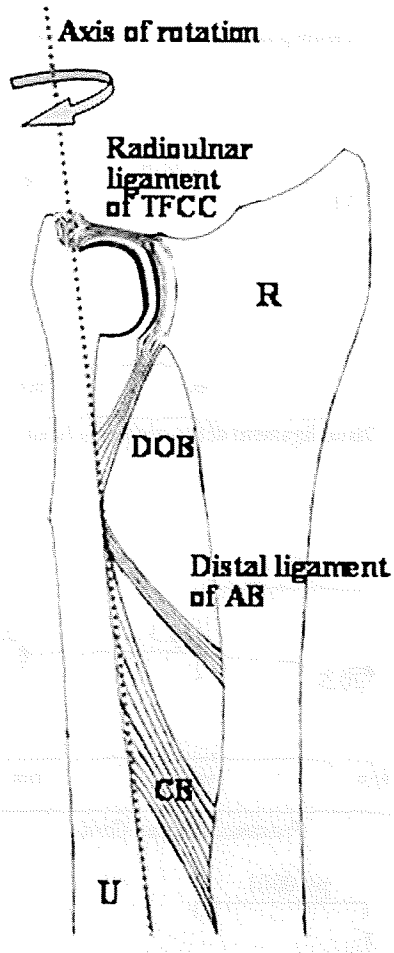

FIGURE 5: Relationship between the distal oblique bundle and the triangular fibrocartilage complex. The DOB appeared to form an isometric collateral ligament with the TFCC to stabilize the forearm during forearm rotation because the ulnar insertions of these ligaments almost coincide with the course of the AOR.

muscles on the IOM may explain why length reduction occurred in pronation.

The DOB is a ligament within the distal membranous portion that we first described in our earlier anatomic study. This ligament is unique because a thick DOB existed in only 40% of the specimens. Originating from around the distal one sixth of the ulnar shaft and inserting into the inferior rim of the sigmoid notch of the radius, the DOB seemed to show continuity with the dorsal and palmar radioulnar ligaments of the TFCC (Fig. 5). The DOB appeared to form an isometric collateral ligament along with the TFCC to stabilize the DRUJ during forearm rotation because ulnar insertions of these ligaments almost coincided with the course of the AOR. The present study revealed that the DOB showed the smallest changes in length during forearm rotation, with the ulnar origin lying on the course of the AOR. We thus hypothesize that the DOB, if it exists, is responsible for stability of the DRUJ during forearm rotation. Several biomechanical studies support our hypothesis. Watanabe et al.[10] suggested that the distal membranous portion is the region that constrains volar and dorsal laxity of the radius at the DRUJ in all forearm rotation positions. Kihara et al.[11] found that subluxation of the DRUJ occurred after the distal membranous portion was cut when the TFCC had been disrupted.

In clinical settings, we often encounter TFCC disruption cases with or without gross instability of the DRUJ and those with or without gross instability of the distal ulnar stump after distal ulnar resection, as described by Darrach.[23] We know that a substantial individual difference exists in the stability of the DRUJ under such pathologic conditions. However, no reasonable explanation for this phenomenon has been suggested. Considering the fact that a thick DOB exists in only 40% of human subjects, we speculate that it acts as a secondary stabilizer of the DRUJ when the TFCC is damaged in patients with a DOB, and stability depends on whether the patient has a DOB. Further biomechanical studies that compare groups with a DOB and those lacking it are required to verify our hypothesis.

Compared with the CB, DOB, and the distal ligament of AB, the proximal oblique cord and dorsal oblique accessory cord did not represent isometric components. The proximal oblique cord is located in the most proximal region of the interosseous space, originating from the anterolateral aspect of the coronoid process of the ulna and inserting just distal to the radial tuberosity. Functions of this ligament are controversial and unconfirmed. Martin[7] and Tubbs et al.[8] stated in their respective cadaveric studies that the proximal oblique cord is lax in the neutral position and pronation but taut in supination. Conversely, Patel[9] reported in his study, using forelimbs of anthropoid primates, that the ligament was lax in the neutral position and supination but became taut in pronation. Our study revealed a dramatic increase in length of the proximal oblique cord in pronation, with the radial attachment out of the course of the AOR, supporting Patel's observations. Thus, the proximal oblique cord is not an isometric component, but is a restraint from excessive pronation motion. This study revealed a gradual increase in length from supination to pronation. The radial attachment was away from the course of the AOR. We therefore suggest that the dorsal oblique accessory cord works as a restraint from excessive pronation motion rather than forming an isometric component.

The current study had limitations. An increase in the length of the ligament in response to an increased load does not indicate that the ligament is tight, because it can increase tension without changing its length. We used attachment location data from the IOM ligaments of cadaver specimens because attachment locations of living subjects cannot be distinguished by imaging.[24–27] Our *in vivo* length measurement of the IOM ligament is likely to be more physiologic than those using cadavers, which lack muscle tone.

In conclusion, distal ligaments (the CB, distal ligament of AB, and DOB) of the IOM appear to form an isometric ligamentous chain to stabilize the forearm during forearm rotation, whereas the proximal ligaments (the proximal oblique cord and dorsal oblique accessory cord) seem to act as restraints from excessive pronation motion of the forearm. The DOB in the distal membranous portion was suggested to stabilize the DRUJ in 40% of human subjects who have this ligament. We hope that this study will prove useful in elucidating the mechanics and pathomechanics of forearm stability.

REFERENCES

1. Skahen JR III, Palmer AK, Werner FW, Fortino MD. The interosseous membrane of the forearm: anatomy and function. J Hand Surg 1997;22A:981–985.
2. Nakamura T, Yabe Y, Horiuchi Y. Functional anatomy of the interosseous membrane of the forearm: dynamic changes during rotation. Hand Surg 1999;4:67–73.
3. Poitevin LA. Anatomy and biomechanics of the interosseous membrane: its importance in the longitudinal stability of the forearm. Hand Clin 2001;17:97–110.
4. Noda K, Goto A, Murase T, Sugamoto K, Yoshikawa H, Moritomo H. The interosseous membrane of the forearm: an anatomical study of ligament attachment locations. J Hand Surg 2009;34A:415–422.
5. Hotchkiss RN, An K-N, Sowa DT, Basta S, Weiland AJ. An anatomic and mechanical study of the interosseous membrane of the forearm: pathomechanics of proximal migration of the radius. J Hand Surg 1989;14A:256–261.
6. Mori K. Experimental study on rotation of the forearm: functional anatomy of the interosseous membrane. The Journal of the Japanese Orthopaedic Association 1985;59:611–622.
7. Martin BF. The oblique cord of the forearm. J Anat 1958;92:609–615.
8. Tubbs RS, O'Neil JT Jr, Key CD, Zarzour JG, Fulghum SB, Kim EJ, et al. The oblique cord of the forearm in man. Clin Anat 2007;20:411–415.
9. Patel BA. Form and function of the oblique cord (*chorda oblique*) in anthropoid primates. Primates 2005;46:47–57.
10. Watanabe H, Berger RA, Berglund LJ, Zobitz ME, An KN. Contribution of the interosseous membrane to distal radioulnar joint constraint. J Hand Surg 2005;30A:1164–1171.
11. Kihara H, Short WH, Werner FW, Fortino MD, Palmer AK. The stabilizing mechanism of the distal radioulnar joint during pronation and supination. J Hand Surg 1995;20A:930–936.
12. Hollister AM, Gellman H, Waters RL. The relationship of the interosseous membrane to the axis of rotation of the forearm. Clin Orthop Relat Res 1994;298:272–276.
13. Goto A, Moritomo H, Murase T, Oka K, Sugamoto K, Arimura T, et al. In vivo three-dimensional wrist motion analysis using magnetic resonance imaging and volume-based registration. J Orthop Res 2005;23:750–756.
14. Crisco JJ, Coburn JC, Moore DC, Akelman E, Weiss AP, Wolfe SW. In vivo radiocarpal kinematics and the dart thrower's motion. J Bone Joint Surg 2005;87A:2729–2740.
15. Moritomo H, Murase T, Goto A, Oka K, Sugamoto K, Yoshikawa H. In vivo, 3-dimensional kinematics of the midcarpal joint of the wrist. J Bone Joint Surg 2006;88A:611–621.
16. Moritomo H, Murase T, Arimitsu S, Oka K, Yoshikawa H, Sugamoto K. The in vivo isometric point of the lateral ligament of the elbow. J Bone Joint Surg 2007;89A:2011–2017.
17. Moritomo H, Murase TArimitsu S, Oka K, Yoshikawa H, Sugamoto K. Change in the length of the ulnocarpal ligaments during radiocarpal motion: possible impact on triangular fibrocartilage complex foveal tears. J Hand Surg 2008;33A:1278–1286.
18. Kinzel GL, Hall AS Jr, Hillberry BM. Measurement of the total motion between two body segments. I. Analytical development. J Biomech 1972;5:93–105.
19. Kinzel GL, Hillberry BM, Hall AS Jr, Van Sickle DC, Harvey WM. Measurement of the total motion between two body segments. II. Description of application. J Biomech 1972;5:283–293.
20. Nakamura T, Yabe Y, Horiuchi Y. In vivo MR studies of dynamic changes in the interosseous membrane of the forearm during rotation. J Hand Surg 1999;24B:245–248.
21. Nakamura T, Yabe Y, Horiuchi Y, Yamazaki N. Three-dimensional magnetic imaging of the interosseous membrane of forearm: a new method using fuzzy reasoning. Magn Reson Imaging 1999;17:463–470.
22. Nakamura T, Yabe Y, Horiuchi Y, Seki T, Yamazaki N. Normal kinematics of the interosseous membrane during forearm pronation-supination: a three-dimensional MRI study. Hand Surg 2000;5:1–10.
23. Darrach W. Partial excision of the lower shaft of the ulna for deformity following Colles' fracture. Ann Surg 1913;57:764–765.
24. Failla JM, Jacobson J, van Holsbeeck M. Ultrasound diagnosis and surgical pathology of the torn interosseous membrane in forearm fractures/dislocations. J Hand Surg 1999;24A:257–266.
25. Starch DW, Dabezies EJ. Magnetic resonance imaging of the interosseous membrane of the forearm. J Bone Joint Surg 2001;83A:235–238.
26. McGinley JC, Roach N, Gaughan JP, Kozin SH. Forearm interosseous membrane imaging and anatomy. Skeletal Radiol 2004;33:561–568.
27. McGinley JC, Roach N, Hopgood BC, Limmer K, Kozin SH. Forearm interosseous membrane trauma: MRI diagnostic criteria and injury patterns. Skeletal Radiol 2006;35:275–281.

JHS(E)

The Journal of Hand Surgery (European Volume, 2009) 34E: 5: 592–597

INTRA-ARTICULAR DISTAL ULNAR FRACTURES ASSOCIATED WITH DISTAL RADIAL FRACTURES IN OLDER ADULTS: EARLY EXPERIENCE IN FIXATION OF THE RADIUS AND LEAVING THE ULNA UNFIXED

J. NAMBA, T. FUJIWARA, T. MURASE, T. KYO, I. SATOH and T. TSUDA

From the Departments of Orthopaedic Surgery, Minoh City Hospital, Ryokufukai Hospital, and Osaka University Graduate School of Medicine, Japan

There is no clear consensus about the best management of intra-articular distal ulnar fractures associated with distal radial fractures in older adults. We describe a treatment wherein the distal radial fractures were securely fixed with a palmar plate, leaving the associated ulnar fractures unfixed. The wrists of 14 patients with a mean age of 74 years were reviewed at an average of 18 months after surgery. The results were excellent in 11 cases and good in three, according to the modified Gartland and Werley score. All fracture sites displayed union, and there was no instability of the distal radioulnar joint. A widening of the distal radioulnar joint space was present in one wrist. Angular deformity of the distal ulnar metaphysis was seen in five wrists. This treatment could be an alternative to open reduction with internal fixation for intra-articular distal ulnar fractures in older adults.

Keywords: ulnar head fracture, conservative treatment, distal radial fracture, distal ulnar fracture

INTRODUCTION

Distal ulnar fractures associated with distal radial fractures are common. There is a consensus regarding the conservative treatment for associated styloid tip or simple neck fractures, which are usually categorised as stable types of fracture (Faierman and Jupiter, 1998; Fernandez and Jupiter, 1996; Geissler et al., 1996; Logan and Lindau, 2008). However, an intra-articular distal ulnar fracture (IADUF) associated with a distal radial fracture has been considered to be potentially unstable because it is an intra-articular fracture and involves a fragment to which the triangular fibrocartilage complex (TFCC) is attached. Open reduction and internal fixation (ORIF) with plates is recommended for IADUF to achieve stabilisation if possible (Faierman and Jupiter, 1998; Fernandez and Jupiter, 1996; Geissler et al., 1996; Logan and Lindau, 2008). However, internal fixation for IADUF is very challenging in older patients due to the poor bone quality and small size of the fracture fragments. For these reasons, various non- or minimally-invasive treatments are preferred for IADUF in older patients in many clinical situations (Biyani et al., 1995). These methods often lead to disappointing results such as a painful distal radioulnar joint (DRUJ) and decreased forearm rotation (Biyani et al., 1995). Currently, there is no clear consensus regarding the appropriate management of associated IADUF in older patients. We have retrospectively reviewed the radiographic and functional results of conservative treatment for IADUF and ORIF with palmar plates for associated ipsilateral distal radial fracture in a group of patients with an average age of 74 years, and we discuss the potential of this treatment in older adults.

PATIENTS AND METHODS

IADUF was defined as the presence of an articular fracture extension of the distal ulnar metaphysis into the ulnocarpal joint or DRUJ with or without associated styloid fractures as seen on plain radiograph or computed tomography. Patients with non-IADUF conditions such as an associated fracture of the tip of the ulnar styloid or simple ulnar neck fracture, and patients younger than 55 years were excluded. Between 2003 and 2007, we treated 14 wrists in 13 female patients (average age 74 years; range 57–93) who had a distal radial fracture and an IADUF in the same wrist. According to the classification of Biyani et al. (1995) (Fig 1), there were five cases of Type 2 (inverted T- or Y-shaped fracture with an ulnar styloid fragment including a portion of the metaphysis) and nine cases of Type 4 (comminuted fracture of lower ulnar metaphysis, with or without styloid fracture) for the distal ulna. Distal radial fractures were classified according to the AO Comprehensive Classification of Fractures (Müller et al., 1990); there were 11 cases of Type A and

three cases of Type C (Table 1). For all distal radial fractures, internal fixation was carried out under general anaesthesia. The distal radius was approached between the radial artery and the flexor carpi radialis tendon with the pronator quadratus being detached, and anatomical reduction of the palmar cortex of the distal radius was accomplished. One nonlocking palmar plate (Matrix plate, Stryker, Inc., USA) for case 1 and 13 palmar fixed-angle plates (Stellar plate, Japan Universal Technologies, Inc., Japan) were used for fixation. Polymethylmethacrylate bone cement (Surgical Simplex P, Stryker, Inc., USA) was used in two wrists, and granules of hydroxyapatite (Bonefill, Mitsubishi Well Pharma, Inc., Japan) was used in one wrist to fill the metaphyseal defect in the distal radius, and consequently maintain anatomical reduction. Reduction of the IADUF was not attempted. In all cases, intraoperative radiographs revealed the absence of any dislocation or subluxation of the DRUJ, and the absence of instability was confirmed with a manual stress test (Nakamura et al., 2004) during surgery. Postoperatively, a palmar splint was applied for 2 weeks while permitting possible rotational motion of forearm. After 2 weeks, the splint was removed, and active and passive mobilisation of the wrist began. All patients were encouraged to carry out finger mobilisation, forearm rotation, and elbow and shoulder movements when splinted, and to move the wrist after the removal of the splint. However, during the early postoperative period, those patients who were judged by the authors to have a risk of contracture received supervised physiotherapy.

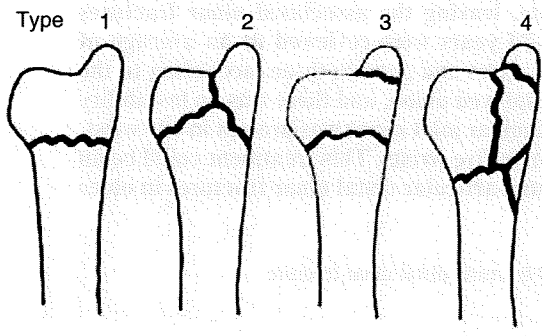

Fig 1 Fracture classification of the distal ulna according to Biyani et al. (1995).

All patients were reviewed clinically and radiographically. The instability of the DRUJ was examined again with the same manual test that was done during the intraoperative examination. The clinical results were assessed according to the system of Gartland and Werley as modified by Sarmiento et al. (1975). In its modified scoring system, the category of nerve complications was expanded to include the ulnar nerve. Range of motion (ROM) was evaluated by recording the degree of flexion-extension and pronation-supination with a standard goniometer. Grip strength was measured by a hand dynamometer (Matsumiya, Co., Ltd., Japan). One patient (case 5) sustained bilateral wrist fractures that

Table 1—Patient demographics and results

			Fracture classification		*ROM*				
Case	*Age*	*Side*	*Radius AO*	*Ulna Biyani*	*E/F*	*P/S*	*Grip strength***	*Functional score****	*Complication*
1	57	L	A2	4	85/75	80/95	96	Excellent	
2	67	L	A3	4	95/70	75/95	89	Excellent	
3	66	R*	A2	2	75/45	90/90	91	Excellent	
4	93	R*	A3	2	65/50	90/90	36	Good	ulnar nerve palsy
5	84	R*	C2	4	50/45	80/65	36#	Good	
		L	A3	4	65/50	50/90	41#	Excellent	
6	77	R*	A3	2	81/67	85/90	100	Excellent	
7	75	L	A3	4	85/60	70/90	78	Excellent	
8	65	L*	A3	2	64/55	70/85	83	Excellent	
9	84	R*	A3	4	66/54	80/90	75	Excellent	
10	76	R*	C3	4	50/55	75/85	43	Good	
11	87	L	A3	4	66/58	80/90	78	Excellent	
12	66	L	C3	4	85/50	90/90	93	Excellent	
13	59	L	A3	2	86/58	80/70	71	Excellent	

*dominant hand.
**% of the contralateral side.
***modified Gartland and Werley scoring system.
#% of the left hand at healthy period before second injury.
E/F = extension/flexion; P/S = pronation/supination.

Table 2—Radiographic results

Case	*RI* (degrees)*	*PT* (degrees)*	*UV* (mm)*	*Time to bone union of the ulnar fracture (weeks)*	*Residual angular deformity of the ulna (degrees)*	*Grade according to modified system of Knirk and Jupiter*
1	25/25	−4/−4	0/0	12	16	1
2	19/20	0/0	0/2	15	nil	0
3	32/30	4/5	1/1.5	12	nil	0
4	23/20	0/0	0/0	7	nil	1
5(R)	30/35	−12/−11	−3/−2	20	9	1
5(L)	28/35	−2/−2	−1.5/−1	12	10	0
6	29/31	15/14	3.5/3	12	nil	0
7	27/30	4/6	−1/1	9	17	1
8	30/29	7/7	−3/−2.5	9	nil	0
9	22/22	13/10	−3/−2	12	nil	0
10	19/22	4/4	−1/0	8	9	1
11	27/30	9/8	2.5/2	12	nil	0
12	23/25	7/9	2.4/1.9	12	nil	0
13	28/26	12/12	0/0	12	nil	0

RI = radial inclination; PT = palmar tilt; UV = ulnar variance.
*immediately postoperatively/at the final follow-up.

had occurred at different times, and sustained the left wrist fracture 2 months after surgery to the damaged right wrist. Preoperative grip strength of the healthy left hand was used for control data. Postoperative radiographs were assessed for fracture union of the distal radius and ulna; the parameters included radial inclination (RI), palmar tilt (PT), ulnar variance (UV) and the change in appearance of the distal ulnar metaphysis and DRUJ. DRUJ arthritis was classified according to the modified criteria of Knirk and Jupiter based on a plain radiograph (Catalano et al., 1997). Fracture healing was defined as bone continuity over the cortical aperture. Radiographic parameters were measured by the Synapse PC-based imaging system (Fujifilm Medical Co., Ltd., Japan).

RESULTS

The mean follow-up time was 18 (range 6–52) months. Five patients (cases 4, 8, 10, 13 and 14) received supervised physiotherapy. At the final outpatient examination, union was evident at all fracture sites in the distal ulna and radius. Postoperative healing of the IADUF was evident at an average of 12 weeks (range 7–20) (Table 2). As assessed using the modified system of Gartland and Werley (Sarmiento et al., 1975), there were 11 excellent and three good results at the final assessment (Table 1). Grip strength was the parameter that showed least improvement in the good cases. Two of three good cases were associated with a Type C fracture of the distal radius.

There was no DRUJ instability in the manual stress test. The average ranges of the wrist and forearm motion were 57° (range 45–75) for palmar flexion, 73° (range 50–95) for extension, 78° (range 45–90) for pronation, and 87° (range 65–95) for supination (Table 1). The average grip strength was 72% of the contralateral side (Table 1). RI, PT and UV on the final radiographs were 27°, 4° and 0.3 mm on average, respectively (Table 2). Widening of the DRUJ space in the coronal plane (5.2 mm) was apparent in case 1 (Fig 2 and Table 2). In this case, atrophy of the distal ulnar metaphysis was thought to be the cause of an apparent horizontal DRUJ gap. In the other cases, atrophy of the distal ulnar metaphysis was not recognised.

Five cases had angulation deformity of the distal ulna in the coronal plane (apex radial) with a mean of 12° (Table 2). In one case (case 6), the alignment of the distal ulnar metaphysis was considered to be gradually reduced during the postoperative period, because an angulation (ulnar apex) of 14° at the immediate postoperative stage had disappeared by final follow-up (Fig 3). With regard to the arthritis grades for the DRUJ, five wrists had grade 1 arthritis (slight narrowing or irregularity of joint space) (Catalano et al., 1997). Four cases (cases 1, 4, 5R, 10) had an irregular articular surface on the ulnar side of the DRUJ and case 7 had a slight narrowing of the DRUJ. Four of five cases with grade 1 arthritis in the DRUJ coincided with the cases with an angulation deformity of the distal ulna (Table 2).

There was one post-surgical complication of ulnar nerve palsy, the symptoms of which were numbness and paraesthesia over the ulnar side of the hand, and a claw deformity (case 4, Table 1). There was a positive Tinel's sign on the ulnopalmar of the wrist which coincided with the IADUF site. This patient had full recovery in the ulnar nerve after surgical release 3 months after operation. From the intraoperative findings, it was

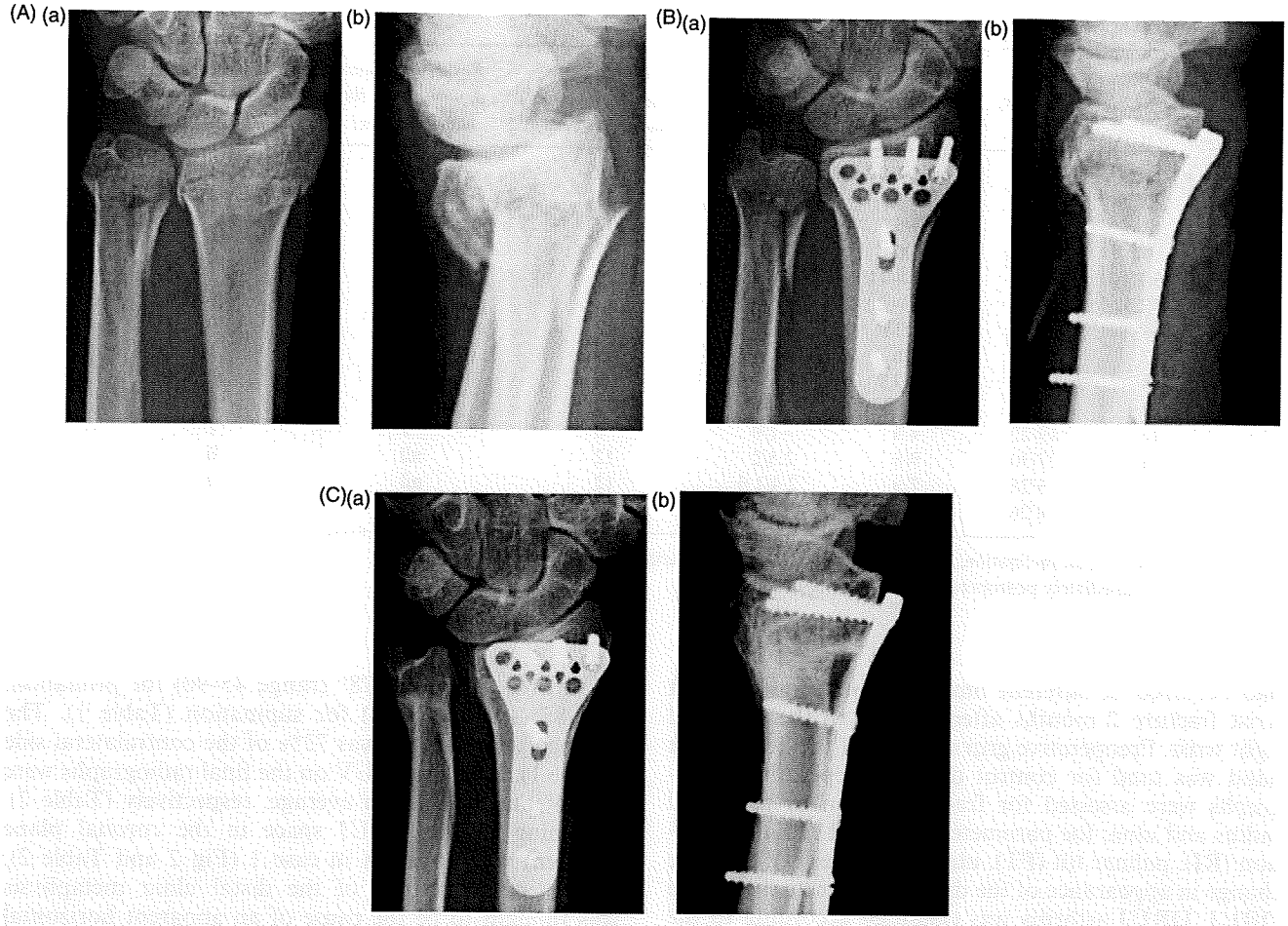

Fig 2 Radiograph of the wrist (case 1). (A) Initial radiograph of the wrist. (B) Radiograph immediately after operation. (C) Final radiograph. All radiographs show (a) anteroposterior and (b) lateral view. The widening of the DRUJ space was apparently due to atrophy of the distal ulnar metaphysis.

believed that scar tissue at the fracture site had entrapped the nerve.

DISCUSSION

There has been little guidance for management of IADUF associated with distal radial fractures. After concomitant distal radial fractures have been stabilised, it has been recommended that the IADUF be stabilised with plates with adequate fixation if possible (Faierman and Jupiter, 1998; Fernandez and Jupiter, 1996; Geissler et al., 1996). Logan and Lindau (2008) stated that operative treatment is not recommended in all cases. Ring et al. (2004) described internal fixation with minicondylar blade plate for five cases of IADUF among 24 distal radial and ulnar fractures in relatively young patients. Dennison (2007) also reported use of the locking plate fixation in three cases of IADUF among five cases of distal radial and ulnar fractures (mean age 52 years). However, in older adult patients, it is quite difficult to fix the fragile osteoporotic fragments with screws and to place hardware on the short nonarticular arc of the distal ulna metaphysis. Biyani et al. (1995) reported on five conservatively treated cases of IADUF among a series of 19 combined distal radial and ulnar fractures. Over 2 mm of ulna plus variance due to axial shortening of the radius was observed in two of the wrists, and callus formation bridging into the DRUJ was observed in one wrist. Their data indicated that the simple conservative method can often lead to ulnocarpal abutment, painful DRUJ arthrosis and a restricted range of forearm rotation.

Excellent stability for distal radial fracture and prevention of radial shortening in the elderly is now possible with the development and success of the palmar fixed-angle plate (Smith and Henry, 2005). Anatomical reduction of the distal radius brings the sigmoid notch (a bony stabiliser of the DRUJ) to its anatomical position, which ensures the stability of the DRUJ.

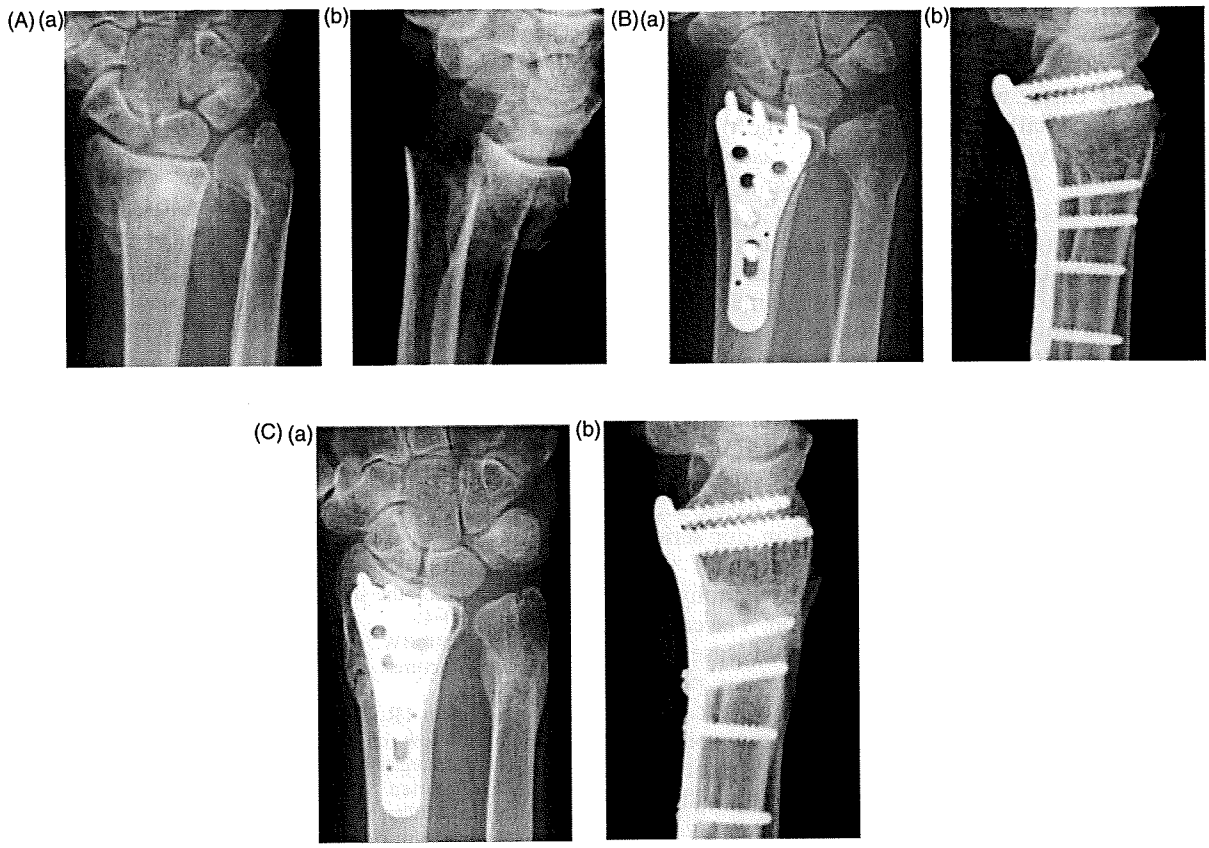

Fig 3 Radiograph of the wrist (case 6). (A) Initial radiograph of the wrist. (B) Radiograph immediately after operation, showing a 14° angulation deformity of the distal ulnar metaphysis (ulnar apex). (C) Final radiograph showing that the angulation apparent at the immediate postoperative stage had disappeared by final follow-up. All radiographs show (a) anteroposterior and (b) lateral view.

We speculated that a realistic approach to resolve the problems of IADUF associated with distal radial fracture in older adults patients would be to make an anatomical and rigid fixation with a palmar plate on the distal radius, while leaving the ulna unfixed, and to begin early wrist mobilisation to avoid stiffness. In this study, we retrospectively reviewed the above-mentioned treatment in 14 cases with older adult patients.

The IADUF seemed to unite easily only if the distal radial fracture was anatomically and rigidly fixed. The surgical techniques of Baldwin's operation (Kersley and Scott, 1990) and the Sauvé-Kapandji method, which aim to create a pseudarthrosis in the distal ulna, are best accompanied by resection of not only the ulnar neck but also the surrounding periosteum to prevent bone regeneration within a periosteal sleeve (Kersley and Scott, 1990; Taleisnik, 1991). It might follow that conservative treatment of the IADUFs in our series, which preserved the periosteum of the ulna whereas the distal radial fracture was surgically stabilised in an anatomical position, would achieve bone union despite early wrist mobilisation.

There was no instability of the DRUJ after surgery. Biyani et al. (1995) surmised that the fractures of the distal radius and ulna might dissipate energy more proximally, thus protecting the carpus, as shown by the absence of carpal injuries in their study. We also considered that an IADUF involving the fragment that attaches the TFCC is not an avulsed fracture, but a comminuted fracture of the distal ulnar metaphysis which maintains the periosteum. Furthermore, the DRUJ is stabilised by bony and soft tissue components such as the sigmoid notch, TFCC (primary stabiliser), extensor carpi ulnaris subsheath, pronator quadratus, and DRUJ capsules (secondary stabilisers) (Gofton et al., 2004). If the sigmoid notch and other secondary stabilisers normally function by reducing the distal radius anatomically, normal DRUJ kinematics are maintained so that the fragment to which TFCC is attached cannot be separated from the fracture site (Gofton et al., 2004).

In contrast, five cases had an angulation deformity of the distal ulnar metaphysis in the coronal plane (apex radial). This phenomenon seems similar to the radioulnar convergence after the Sauvé-Kapandji procedure, which can be induced by traction forces from the muscles of the

first dorsal compartment and the interosseous membrane (Inagaki et al., 2006). The IADUF united while the proximal part of the ulna was being pulled by muscles in some of our cases, which resulted in an angulation deformity (apex radial). We consider that the transient angulation deformity (apex ulnar) in one case (case 6) changed to a nil angulation for the same reason. Consistent with this, Dennison (2007) also reported a residual angulation (apex radial) of a maximum of 8° in his series, including fractures of the distal ulnar shaft. In our cases, angular malunion of the distal ulnar metaphysis did not affect the range of forearm rotation.

Regarding the DRUJ incongruency, the final radiographic parameters were well preserved when compared to postoperative ones. In this study, the average ulnar variance was 0.3 mm positive which led to the absence of an ulnocarpal abutment (Table 2). However, there was irregularity of the articular surface in four cases, and slight narrowing in one case in the DRUJ in our series (Table 2). One case (case 1) showed widening of the DRUJ space due to the atrophy of the ulnar metaphysis, which appeared similar to DRUJ dissociation. The cause of the atrophy is unknown; however, only in this case was the distal radius fixed with a nonlocking palmar plate, whereas fixed-angle plates were used in all the other cases.

There was one complication of ulnar nerve palsy. Although it is unknown if the present method is likely to produce ulnar nerve injury, careful monitoring will be required to detect its occurrence in future cases.

Our study demonstrates that for IADUF associated with distal radial fractures, bone union with functionally satisfactory results can be achieved only if the distal radial fractures are anatomically and rigidly fixed. All patients reported good function in the forearm and wrist, and no patient noted pain in the DRUJ or restrictions in work or daily activities. The drawback is the radiographic problem of early degenerative arthritis of the DRUJ and angulation deformity of the distal ulnar metaphysis. Therefore we do not recommend its primary use in young patients.

Although the number of cases reported here is small, the results are encouraging. When ORIF of the IADUF is not a viable option, this treatment might be a good alternative, especially in older adult patients.

References

Biyani A, Simison AJ, Klenerman L. Fractures of the distal radius and ulna. J Hand Surg Br. 1995, 20: 357–64.

Catalano 3rd LW, Cole RJ, Gelberman RH, Evanoff BA, Gilula LA, Borelli J. Displaced intra-articular fractures of the distal aspect of the radius. Long-term results in young adults after open reduction and internal fixation. J Bone Joint Surg Am. 1997, 79: 1290–302.

Dennison DG. Open reduction and internal locked fixation of unstable distal ulna fractures with concomitant distal radius fracture. J Hand Surg Am. 2007, 32: 801–5.

Faierman E, Jupiter JB. The management of acute fractures involving the distal radio-ulnar joint and distal ulna. Hand Clin. 1998, 14: 213–29.

Fernandez DL, Jupiter JB. Epidemiology, mechanism, classification. In: Fernandez DL, Jupiter JB (Eds.) *Fractures of the distal radius. A practical approach to management*. New York, Springer-Verlag, 1996: 48–50.

Geissler WB, Fernandez DL, Lamey DM. Distal radioulnar joint injuries associated with fractures of the distal radius. Clin Orthop Relat Res. 1996, 327: 135–46.

Gofton WT, Gordon KD, Dunning CE, Johnson JA, King GJW. Soft-tissue stabilizers of the distal radioulnar joint: an in vitro kinematic study. J Hand Surg Am. 2004, 29: 423–31.

Inagaki H, Nakamura R, Horii E, Nakao E, Tatebe M. Symptoms and radiographic findings in the proximal and distal ulnar stumps after the Sauvé-Kapandji procedure for treatment of chronic derangement of the distal radioulnar joint. J Hand Surg Am. 2006, 31: 780–4.

Kersley JB, Scott BW. Restoration of forearm rotation following malunited fractures: Baldwin's operation. J Hand Surg Br. 1990, 15: 421–4.

Logan AJ, Lindau TR. The management of distal ulnar fractures in adults: a review of the literature and recommendations for treatment. Strategies Trauma Limb Reconstr. 2008, 3: 49–56.

Müller ME, Nazarian S, Koch P, Schatzker J. Radius/ulna, distal segment. In: Müller ME, Nazarian S, Koch P, Schatzker J. (Eds.) *The comprehensive classification of fractures of long bones*. Berlin, Springer-Verlag, 1990: 106–15.

Nakamura T, Nakao Y, Ikegami H, Sato K, Takayama S. Open repair of the ulnar disruption of the triangular fibrocartilage complex with double three-dimensional mattress suturing technique. Tech Hand Up Extrem Surg. 2004, 8: 116–23.

Ring D, McCarty LP, Campbell D, Jupiter JB. Condylar blade plate fixation of unstable fractures of the distal ulna associated with fracture of the distal radius. J Hand Surg Am. 2004, 29: 103–9.

Sarmiento A, Pratt GW, Berry NC, Sinclair WF. Colles' fractures. Functional bracing in supination. J Bone Joint Surg Am. 1975, 57: 311–7.

Smith DW, Henry MH. Volar fixed-angle plating of the distal radius. J Am Acad Orthop Surg. 2005, 13: 28–36.

Taleisnik J. The Sauvé-Kapandji procedure. Clin Orthop Relat Res. 1991, 275: 110–23.

Received: 26 November 2008
Accepted after revision: 2 February 2009
J. Namba, MD, PhD, Department of Orthopaedic Surgery, Minoh City Hospital, 5-7-1, Kayano, Minoh, Osaka 562-8562, Japan. Tel.: +81-72-728-2001; fax: +81-72-728-8232.
E-mail: bpdum202@tcct.zaq.ne.jp.

doi: 10.1177/1753193409103728 available online at http://jhs.sagepub.com

SCIENTIFIC ARTICLE

Interosseous Membrane of the Forearm: An Anatomical Study of Ligament Attachment Locations

Kazuo Noda, MD, Akira Goto, MD, PhD, Tsuyoshi Murase, MD, PhD, Kazuomi Sugamoto, MD, PhD, Hideki Yoshikawa, MD, PhD, Hisao Moritomo, MD, PhD

Purpose The interosseous membrane (IOM) of the forearm is a stout ligamentous complex that reportedly comprises several ligamentous components. The purpose of this cadaveric study was to define all IOM ligaments and to clarify the precise attachment locations.

Methods Thirty forearms from 15 embalmed cadavers were used. After dissection, all IOM ligaments were identified, and attachments were measured from the tip of the radial styloid or the ulnar head. Attachment locations were represented as a percentage of total bone length from the distal end of the radius or ulna.

Results The IOM included 5 kinds of ligaments: central band, accessory band, distal oblique bundle, proximal oblique cord, and dorsal oblique accessory cord. The most distal and proximal ends of the radial origin of the central band were 53% and 64% of total radial length from the tip of the radial styloid, whereas those of the ulnar insertion were 29% and 44% of total ulnar length from the ulnar head. The center point of the radial origin and ulnar insertion of the accessory band were 37% and 23%, respectively. The center points of the ulnar origins and radial insertions were 15% and 10% for the distal oblique bundle; 80% and 79% for the proximal oblique cord; and 64% and 62% for the dorsal oblique accessory cord, respectively.

Conclusions The present study clarified precise attachment locations of all representative IOM ligaments. This information will be useful in planning proper graft placement in ligament reconstruction surgery and for future biomechanics research into the function of the IOM ligaments. *(J Hand Surg 2009;34A:415–422. © 2009 Published by Elsevier Inc. on behalf of the American Society for Surgery of the Hand.)*

Key words Anatomy, attachment location, forearm, interosseous membrane (IOM), ligament.

THE INTEROSSEOUS MEMBRANE (IOM) of the forearm is a stout ligamentous complex linking the radius to the ulna. The anatomy of this structure has been studied by various investigators.[1–7] The IOM reportedly consists of distal membranous, middle ligamentous, and proximal membranous portions. Each portion is also known to include several ligamentous components. The most representative component of the IOM is called the central band (CB),[1,2] the broadest and stoutest collection of fibers in the IOM, running obliquely from the proximal radial shaft to the distal ulnar shaft. Prior biomechanical studies[1–3,8–11] have revealed that the CB plays important roles in maintaining forearm functions, as the longitudinal stabilizer of the forearm, and as a load transmitter between the radius and ulna.

The other components of the IOM reportedly comprise the accessory band (AB),[2] which is located adjacent to the CB; the proximal oblique cord[4,5,12–15] on the anterior aspect of the forearm; and the dorsal oblique accessory cord[5] on the posterior side. Some confusion seems to exist with regard to the terminology because prior authors have often used their own terms to repre-

From the Department of Orthopaedic Surgery, Osaka University Graduate School of Medicine, Suita, Osaka, Japan.

Received for publication April 18, 2008; accepted in revised form October 27, 2008.

No benefits in any form have been received or will be received related directly or indirectly to the subject of this article.

Corresponding author: Hisao Moritomo, MD, PhD, Osaka University Graduate School of Medicine, 2-2 Yamadaoka, Suita, Osaka 565-0871, Japan; e-mail: moritomo@ort.med.osaka-u.ac.jp.

0363-5023/09/34A03-0006$36.00/0
doi:10.1016/j.jhsa.2008.10.025

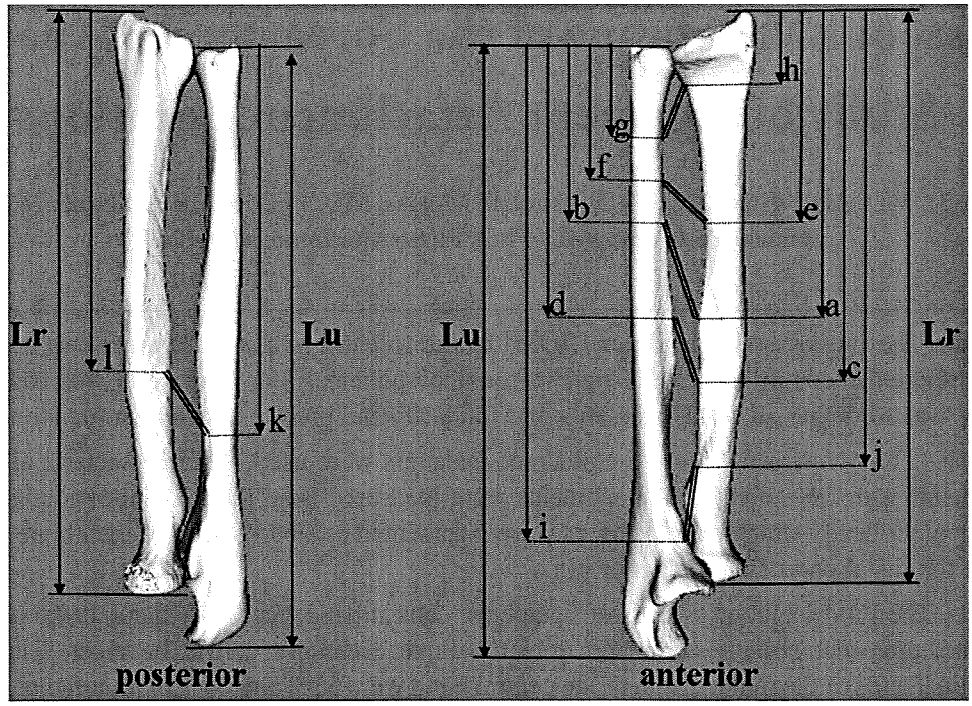

FIGURE 1: Measurement of attachment locations of IOM ligaments. Lr, radial length; Lu, ulnar length. a to l, lengths from the tip of the radial styloid for the radius or from the ulnar head for the ulna. Attachment locations are expressed as percentages of total bone length from the distal end (e.g., a/Lr ×100). a, b and c, d, distal and proximal ends of the central band; e, f, distal ligament of the accessory band; g, h, distal oblique bundle; i, j, proximal oblique cord; k, l, dorsal oblique accessory cord.

sent these structures, and the functions of these ligaments remain a mystery.

IOM researchers have documented the morphological characteristics of the IOM ligaments well, including measurements such as width,[1,2,4,5] thickness,[1,5,6] and insertion angle of the ligament into the radius and ulna.[2,7,16] The purpose of this study was to define all IOM ligaments and to clarify precise attachment locations.

MATERIALS AND METHODS

Thirty forearms from 15 embalmed cadavers (9 females, 6 males) were examined for the width, thickness, and attachment location of the IOM ligaments. Mean age at time of death was 85 years (range, 60–96 years). No apparent pathological lesions were identified in the forearms. The upper extremities were amputated at the middle of the upper arms. Specimens were carefully stripped of all soft tissues remaining on IOM structures and capsuloligamentous tissues around the wrists and elbows. The measurements were made with the forearm positioned in neutral rotation. The width and thickness of each IOM ligament was measured using calipers (accuracy, 0.05 mm; Mitutoyo, Kanagawa, Japan). We then identified the origins (proximal attachments) and insertions (distal attachments) of all ligaments. The locations of the attachments were measured from the tip of the radial styloid for the radius and from the ulnar head for the ulna (Fig. 1). For the CB, both the distal and proximal ends of attachment were measured because it had a broad attachment. For the other ligaments, only the center points of the attachments were measured because they had narrow attachments. A stainless steel ruler (accuracy, 0.15 mm; Shinwa Rules, Niigata, Japan) was used for location measurement. Attachment locations were expressed as percentages of the total bone length of the radius or the ulna from each distal end.

RESULTS

Middle ligamentous complex

The middle portion of the IOM (the middle ligamentous complex) was a complex of ligaments that were quadrilateral in shape and were located within the interosseous space. The middle ligamentous complex was further divided into 2 ligamentous components, the CB and the AB.

Central band: The widest and thickest ligament was the CB, forming part of the middle ligamentous complex (Figs. 2–5). The CB originated from the interosseous

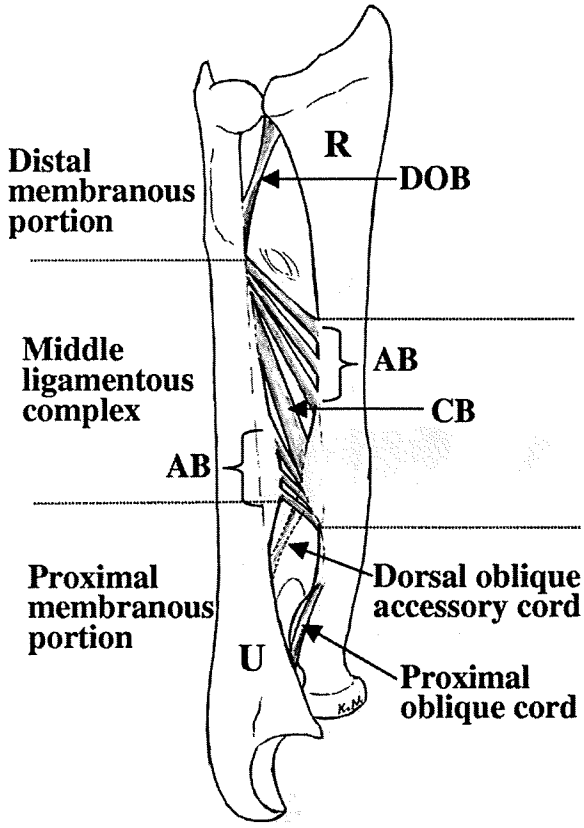

FIGURE 2: Schematic structure of the IOM. Right forearm viewed from the anterior aspect. The IOM consists of distal, middle, and proximal portions. The middle portion is a ligamentous complex (middle ligamentous complex) that is further divisible into the CB and the AB. Distal and proximal portions on either side of the middle portion comprise transparent membranous tissue (distal and proximal membranous portions) with holes for perforation of the interosseous artery. The DOB is present within the distal membranous portion. The proximal oblique cord is present on the anterior side of the forearm and the dorsal oblique accessory cord on the posterior side in the proximal membranous portion. R, radius; U, ulna.

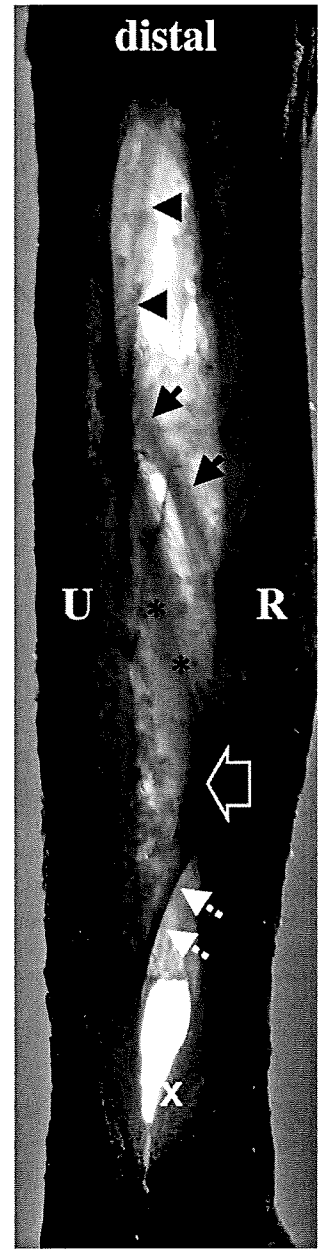

FIGURE 3: Backlit photograph of IOM ligaments. Asterisks indicate the CB as part of the middle ligamentous complex, which originates from the interosseous crest of the radius (white arrow), runs distally and ulnarly, and inserts into the interosseous border of the ulna. Arrows indicate the AB, which runs in a similar way to the CB. Arrowheads indicate the DOB within the distal membranous portion, which originates from around the distal one sixth of the ulnar shaft and inserts into the inferior rim of the sigmoid notch of the radius. Broken arrows indicate the dorsal oblique accessory cord on the posterior aspect of the forearm, which originates from around the distal two thirds of the ulnar shaft and inserts into the interosseous crest of the radius. The proximal oblique cord cannot be distinguished in this photograph because this cord is in contact with the surface of the radial tuberosity (x). R, radius; U, ulna.

crest of the radius, which is the interosseous ridge of the radius that projects most ulnaward, then coursed distally and ulnarly and inserted into the interosseous border of the ulna. The CB was seen in all specimens. The mean width was 9.7 ± 3 mm (range, 4.4–16 mm) measured perpendicular to its fibers, and the mean thickness was 1.3 ± 0.2 mm (range, 1–1.6 mm). The locations of the attachments of the CB on the radius and ulna are detailed in Table 1.

Accessory band: Several ligaments, which were in the same coronal plane as the CB, existed on either side of the CB in the middle ligamentous complex and were collectively termed the AB (see Figs. 2, 3). The fibers of the AB ran in almost the same direction as the CB